



Sharif University of Technology
Scientia Iranica
Transactions A: Civil Engineering
<http://scientiairanica.sharif.edu>



The effects of period and nonlinearity on energy demands of MDOF and E-SDOF systems under pulse-type near-fault earthquake records

S.A. Razavi^a, N. Siahpolo^{a,b,*}, and M. Mahdavi Adeli^a

a. *Department of Civil Engineering, Ahvaz Branch, Islamic Azad University, Ahvaz, Iran.*

b. *Department of Civil Engineering, Institute for Higher Education ACECR, Khouzestan, Iran.*

Received 13 March 2020; received in revised form 19 October 2020; accepted 16 November 2020

KEYWORDS

Energy demand;
 MDOF systems;
 SDOF systems;
 Pulse-type near-fault earthquake;
 Higher modes effects.

Abstract. The use of an earthquake input energy concept and types of internal energy in structures has been less considered for near-fault pulse-like earthquakes. This paper calculates the applied ratios of energy types in the E-SDOF and MDOF systems and identifies the relationship between them. For this purpose, five steel frames (4, 10, 15, 20, and 30 story steel MRFs with 3-span) were designed, and the E-SDOF structure was obtained equivalent to the first mode, using the Modal Pushover Analysis (MPA) method. All models were analyzed under 10 near-fault pulse-like earthquake records using nonlinear time history analysis. The results show that the Total Dissipated Energy (TDE) of the structure depends on its nonlinear degree and period. The TDE of the MDOF and E-SDOF systems is equal for long periods, and its size is independent of the design resistance (R) and the degree of nonlinearity. However, during short periods, this ratio is close to the effective modal mass coefficient corresponding to the first mode. The story normalized hysteretic energy ratio is also a function of the height, nonlinear degree; and period of the structure. In addition, the effect of higher modes affects the distribution of this ratio in tall structures.

© 2021 Sharif University of Technology. All rights reserved.

1. Introduction

Throughout the past few decades, energy-based methods have been devised in earthquake engineering, and are currently applied in design optimization [1]. Some researchers proposed the application of energy methods for the seismic design [2,3], as well as for designing the moment frames [4,5]. Nevertheless, the most prominent

study that established the concepts of the input and output energies as measures of structural damage was conducted by Uang and Bertero [2]. Their study indicated the importance of absolute input energy and considerable increase of energy in the input energy time history. Thereafter, numerous studies have been carried out to accurately estimate the energy demands and energy dissipation mechanisms in structures.

The energy-based design approach is based on the argument that the energy dissipation capacity of structural elements can be calculated using the energy demand estimated under the effect of an earthquake. Goel et al. proposed a Performance-Based-Plastic Design (PBSD) method with the energy factor of

*. *Corresponding author.*
E-mail addresses: siahpolo@acecr.ac.ir and n.siahpolo@gmail.com (N. Siahpolo)

elastic-plastic SDOF systems quantifying the seismic demand [6]. The effectiveness of this method has been examined by applying the procedure in steel moment resisting frames [7], steel frames with buckling restrained braces [8], braced truss moment frames [9,10], and steel frames with steel shear walls [11].

It was also observed that the energy factor represents as a reliable demand index for quantification of peak response demand of an innovative system (i.e. damage-control structures with energy dissipation fuses) [12,13,14].

Near-faults ground motion is substantially influenced by faulting mechanisms, strike, and rupture directivity depending on the site (e.g. forward directivity) and the permanent static deformation at the fault, which is known as the Fling Step. Hence, because of the near-fault earthquake parameters, the significant energy of rupture manifests as a long period pulse-type excitation. Such a pulse-type ground motion is often observed at the beginning of the acceleration time history and tends to increase the acceleration response spectrum over long periods. In this case, a considerable amount of the earthquake energy dissipates with slight long-amplitude pulses, and significant demands are imposed on the structure. Thus, the risk of brittle fracture grows in structural elements of poor construction details. The effects of this phenomenon were observed during the Arzakan (1992), Landers (1992), Northridge (1994), Great Hanshin (1995), Kocaeli (1999), and Chi-Chi (Taiwan) earthquakes.

The ease of using spectra is a key and useful tool for design engineers. Therefore, the preparation of the relative input energy spectrum causes the use of energy criteria in the seismic design of structures to be accompanied by higher success by structural designers. Du et al. presented a compatible energy demand estimate, based on the input energy spectra and the hysteretic-to-input energy ratio design spectra consistent with code, to make the hysteretic energy demand estimate in the energy-based seismic design approach consistent with current seismic design [15]. Yang et al. adopted a design method, named the equivalent energy design procedure, to design the EBF systems. The introduced method is an alternative design procedure for fused structural systems, where engineers can design the structure to achieve the intended performance objectives at different earthquake hazard levels. Unlike conventional force-based design methodologies, the newly developed algorithm does not require the assumption of response modification factors or the fundamental period of a structure in the design procedure [16]. Regarding improvement in the seismic performance of high-speed railway bridges, Guo et al. adopted the friction pendulum bearing. They present an improved energy-based design procedure, which considers multiple performance objectives, and takes

the post-yield stiffness into account. Besides, they verified the improved method by numerical examples [17]. Oh et al. verified the acceleration response spectrum according to structural characteristics by numerical analysis and compared it to the stability of the energy response spectrum. They showed that the energy response spectrum is appropriate for the design of a vibration control structure in which the distributions of the stiffness and strength change rapidly, including seismic structures [18]. Zhou et al. proposed an approach to predict the hysteretic energy demand for self-centering single-degree-of freedom systems [19]. Also, Zhou et al. illustrate that although ground motion types have little influence on the EH/EI spectra, both structural features, including energy ratio, damping ratio, and ductility factor, and the initial period of systems, play a significant role in the determination of the EH/EI spectra [20]. Sen and Gupta estimated the seismic damage in frame-type multi-degree-of-freedom systems using the results of linear response instead of nonlinear response. The proposed methodology is based on the assumption that seismic damage in a system can be estimated by computing the damage index in each of the equivalent oscillators corresponding to the modes of linear vibration and by combining those damage indices through a combination rule. It has also been assumed that the hysteretic properties of the equivalent oscillators can be estimated from the nonlinearity characteristics of the beam and column sections of the frame. An estimation of the damage index in each of the equivalent oscillators has been carried out using the linear displacement peaks exceeding the yield level, together with the models for ductility demand ratio and normalized hysteretic energy demand. Yang et al. presents an equivalent energy design procedure for the seismic design of fused structures. They showed that the procedure can have a controlled degree of damage at the designated elements [21]. Vahdani et al. showed that changes of ξ and μ do not have a significant effect on the overall shape of the spectrum and its values in the field of inelastic behavior and in a wide range of periods, except near the peak of the spectra. But, in the area of inelastic behavior, the effect is greater. For engineering purposes, it can be said that the input energy per unit mass of the structure is almost independent of the damping ratio and ductility of the structure, and is a function of the periodicity of the structure [22].

Benioff (1955) presented a report of the most important properties of near-fault earthquakes using the intensity patterns generated during the Kern County earthquake [23]. Later on, Mahin et al. [24] and Bertero et al. [25] studied the structural damage caused by the pulse-type nature of the near-fault San Fernando earthquake (1971). Hall et al. indicated that the displacement caused by the pulses of near-fault

earthquakes imposes considerable seismic demand on structures [26]. Krawinkler et al. assessed a steel moment-resisting frame under the effect of a near-fault earthquake and stated that the structural response to the persistence of the acceleration pulse, which matches the fundamental period, is critical [27].

On the other hand, many researchers have investigated the effects of this pulse-type ground motion on the linear and nonlinear behavior of SDOF systems [28].

Based on the aforementioned literature review, less attention has been paid to the effect of near-fault earthquakes with pulse-type velocity and acceleration time history on the energy content (imposed and dissipated energy). Further, quantification of energy demand, both for SDOF and MDOF systems, under pulse-type motions is another shortcoming of previous studies. It seems that the relationship between the energy demand of SDOF and MDOF systems can be the basis of a new method in seismic design. Thus, this study focuses on calculating different types of energy, including the energy dissipated due to cyclic behavior, damping energy, and elastic strain energy. Also, the total dissipated energy, which almost equals the input energy at the end of the ground motion, is another energy demand investigated in this study. The calculations were carried out for SDOF and MDOF structures. Then, in order to explain the effects of the MDOF system on energy demand, the MDOF energy demand ratio was divided by the SDOF energy demand ratio. According to these ratios, a simple process can be established for calculating the maximum energy of an MDOF system using SDOF energy. To this end, five 2D steel moment frames with heights of 4, 10, 15, 20, and 30 stories have been designed according to the Iran seismic design code. The aforementioned energy demands and the dissipated energy at the stories of the structural models have been determined via nonlinear dynamic analysis under 10 pulse-type earthquake ground motions. Then, the results have been investigated both for MDOF and corresponding SDOF systems.

2. Basic formulation of the SDOF system input energy

For a SDOF system with known dynamic characteristics subjected to earthquake acceleration time history, integrating the equation of motion with respect to a displacement (u) yields the absolute energy as follows:

$$E_K + E_\zeta + (E_S + E_H) = E_{AI}. \quad (1)$$

Eq. (1) includes different types of energy components:

$$E_K = m \frac{(\dot{u} + \dot{u}_g)^2}{2}, \quad (2)$$

$$E_\zeta = \int (c\dot{u})du, \quad (3)$$

$$E_S + E_H = \int f(u)du, \quad (4)$$

$$E_{AI} = \int m(\ddot{u}_g + \ddot{u})\dot{u}_g dt. \quad (5)$$

In this equation, E_{AI} , E_K , E_ζ , E_S , and E_H are the absolute input energy, absolute kinetic energy, damping energy, elastic strain energy, and plastic strain energy (i.e. non-renewable hysteretic energy or HE), respectively. Meanwhile, the relative energy of the SDOF system could be rewritten as follows:

$$E_{KR} + E_\zeta + (E_S + E_H) = E_{RI}, \quad (6)$$

where, E_{RI} and E_{KR} denote relative input energy and relative kinetic energy, respectively.

$$E_{KR} = m \frac{\dot{u}^2}{2}, \quad (7)$$

$$E_{AI} = - \int m\ddot{u}_g \dot{u} dt. \quad (8)$$

E_{AI} represents work done on the structure by the inertia force ($m\ddot{u}_t$) which is equivalent to the work exerted by the total base shear force under the ground motions. The work done by the fixed-base structure under equivalent lateral load is denoted by E_{RI} . It is apparent that this energy does not include the rigid body motion effect. Since in Eqs. (1) and (6), the damping energy, elastic strain energy, and plastic strain energy are the same, the difference between the absolute and relative kinetic energies yields the distinction between these two energies.

$$E_{AI} - E_{RI} = E_K - E_{KR} = \frac{1}{2}m\dot{u}_g^2 + m\dot{u}_g \dot{u}. \quad (9)$$

The first and second terms on the right side of Eq. (9) indicate the kinetic energy under the effect of ground velocity and the work done by the ground acceleration with respect to the gradual rise in structural displacement, respectively. It could initially be argued that the absolute and relative energy inputs of the extremely rigid and extremely soft structures are different. In flexible (soft) structures, where the natural period of vibration is larger than the predominant period of the ground motion, the mass of structure remains in its initial position, while the foundation of the structure experiences a movement equal to the ground motion, simultaneously. In this case, the absolute input energy acting on the structure is zero, while there is a considerable relative energy exerted onto the structure. On the contrary, the relative mass displacement with respect to the ground is trivial in rigid structures. As a result, the relative input earthquake energy is almost zero and a considerable absolute energy acts on the structure.

Table 2. Column section properties.

Section name	Section ID	Flange width b_f (mm)	Flange thickness t_f (mm)	Web height h_w (mm)	Web thickness t_w (mm)
BOX 200X15	C1	200	15	200	15
BOX 250X15	C2	250	15	250	15
BOX 300X25	C3	300	25	300	25
BOX 350X30	C4	350	25	350	25
BOX 350X30	C5	350	30	350	30
BOX 400X30	C6	400	30	400	30
BOX 450X30	C7	450	30	450	30
BOX 500X40	C8	500	40	500	40
BOX 550X40	C9	550	40	550	40
BOX 600X40	C10	600	40	600	40
BOX 650X40	C11	650	40	650	40

Table 3. Beam section properties.

Section name	Section ID	Flange width b_f (mm)	Flange thickness t_f (mm)	Web height h_w (mm)	Web thickness t_w (mm)
TW300F150TH15	B1	150	15	300	15
TW350F150TH15	B2	150	15	350	15
TW400F200TH15	B3	200	15	400	15
TW450F200TH15	B4	200	15	450	15
TW500F250TH15	B5	250	20	500	20
TW550F250TH20	B6	250	20	550	20
TW600F300TH20	B7	300	20	600	20
TW600F350TH20	B8	350	20	600	20

were carried out on the frames using ETAB2016 software [32]. The frames were designed using the Load and Resistance Factor Design (LRFD) method [33]. The ETABS2016 model assumes rigid full-strength beam column connections, rigid full-strength column bases, and a horizontal diaphragm constraint for the nodes of each floor to account for the in-plane rigidity of the composite slab. Besides of designing the frames using the resistance factor, distribution of stiffness along the height was adjusted to limit the maximum inter-story drift angle to the allowable levels specified in Standard 2800.

3.2. Models for nonlinear dynamic analysis and near-fault ground motions

The OpenSEES software [34] can be used to develop nonlinear models for the steel MRFs. Beams are modeled as displacement-based fiber elements. Each fiber was assumed to exhibit uniaxial bilinear elasto-plastic stress-strain cyclic behavior. Panel zones were considered rigid and elastic. Force-based fiber elements were used to model the columns to accurately capture moment-axial force interaction effects. Further, to ac-

count for the axial rigidity of the composite slab, a rigid diaphragm constraint was imposed at the nodes of each floor, while to capture the $P - \Delta$ effects of the gravity loads acting in the tributary plan area of the steel MRF, the *Corotational Coordinate Transformation* was included in the models. To integrate the equations of motion of the steel MRFs subjected to earthquake ground motion, the Newmark method with constant acceleration was used. To minimize the unbalanced forces within each integration time step, the Newton method with tangent stiffness was employed, while an automatic technique of decreasing the time step was utilized to overcome convergence issues. The inherent 5% damping ratio at the first two modes of vibration were modeled using a Rayleigh damping matrix that excludes from its stiffness proportional component all the nonlinear springs with high initial stiffness so that large damping forces can be avoided. A nonlinear force-controlled static analysis was first performed under the gravity loads of the seismic design combination and then nonlinear dynamic analysis was conducted.

Baker presented a general definition of the distinctive characteristics of near-fault earthquakes [35].

Table 4. Records of 10 near-fault earthquakes with forward directivity effects.

Record no.	Earthquake name	Year	Station name	PGA (g)	Mw	R (km)	T_P (s)
1	Loma Prieta	1989	Gilroy - Gavilan Coll.	0.25	6.93	9.96	1.79
2	Northridge-01	1994	Newhall - Fire Sta	0.18	6.69	5.92	1.03
3	Northridge-01	1994	Newhall - W Pico Canyon Rd.	0.33	6.69	5.48	2.40
4	Northridge-01	1994	Rinaldi Receiving Sta	0.08	6.69	6.50	1.23
5	Northridge-01	1994	Sylmar - Converter Sta East	0.58	6.69	5.19	3.52
6	Kocaeli, Turkey	1999	Gebze	0.30	7.51	10.92	5.78
7	Landers	1992	Yermo Fire Station	0.10	7.28	23.62	7.50
8	Morgan Hill	1984	Coyote Lake Dam (SW Abut)	0.23	6.19	0.53	0.95
9	Kobe, Japan	1995	KJMA	1.05	6.90	0.96	0.95
10	Kobe, Japan	1995	Takarazuka	0.94	6.90	0.27	1.42

According to this definition, a near-fault earthquake must meet the following three requirements.

- Pulse index must be higher than 0.85;
- Pulse must be formed in the early seconds of velocity time history;
- PGV of the earthquake record must be higher than 30 cm/sec.

Based on the aforementioned three criteria, 91 earthquake records fall under the category of near-fault earthquakes [35]. One of the most important attributes of the near-fault pulses is the velocity pulse period. Baker proposed to convert the initial acceleration time history to a set of decomposed acceleration time histories through wavelet analysis. Afterwards, the acceleration time history with the highest wavelet transform coefficient was identified, and subsequently the velocity response spectrum was obtained using this acceleration time history. The point at which spectral velocity in the horizontal direction peaks would indicate the predominant pulse period. The findings of Baker's study also showed that the pulse period obtained through the abovementioned method was close to the pulse period observed in the velocity time history [35].

According to Baker's proposed method, 10 fault-perpendicular components were selected among the 91 pulse-type near-fault ground motions, which show the forward directivity. Details of these records, denoted by NF-SP, are listed in Table 4.

3.3. Equivalent SDOF system

In this study, the Modal Pushover Analysis (MPA) [36] method was used to develop the characteristics of the Equivalent SDOF (E-SDOF) system. Only the first mode of vibration (fundamental mode) was considered. For this purpose, initially, the natural frequency and mode shape of steel MRFs was calculated by eigenvalue analysis. Then, the capacity curve (shear-roof

displacement) was developed for the first mode force distribution.

$$S_1^* = m\phi_1, \quad (10)$$

where, m is the mass matrix of the structure and ϕ_1 denotes the first mode shape vector. Next, the capacity curve was idealized as a bilinear pushover curve, called the elasto-plastic curve. Then, the idealized pushover curve was converted to a first mode force-displacement ($F_{s1}/L_1 - D_1$) inelastic SDOF system by utilizing Eq. (11).

$$\frac{F_{S1}}{L_1} = \frac{V_{b1}}{m_1^*}, \quad (11)$$

$$D_{1y} = \frac{u_{r1y}}{\Gamma_1 \varphi_{r1}}, \quad (12)$$

where, m_1^* is the effective modal mass and φ_{r1} is the value of φ_1 at the roof, and:

$$\Gamma_1 = \frac{\phi_1^T m_1}{\phi_1^T m \phi_1}. \quad (13)$$

Finally, the elastic vibration period of the system is:

$$T_1 = 2\pi \sqrt{\frac{L_1 D_{1y}}{F_{S1y}}}. \quad (14)$$

For a SDOF system with known T_1 and ζ_1 , inelastic demands can be computed by nonlinear response history analysis or from the inelastic design spectrum.

3.4. Research methodology

Following the initial analysis, design, and determining the sections, the models introduced in Section 3.1 were used to generate the practical ratios through analysis. To this end, initially, the target behavior coefficient ($R_{t,i}$) was set to 0.25, 0.5, 0.75, and 1 in the elastic analyses. This coefficient was considered equal to

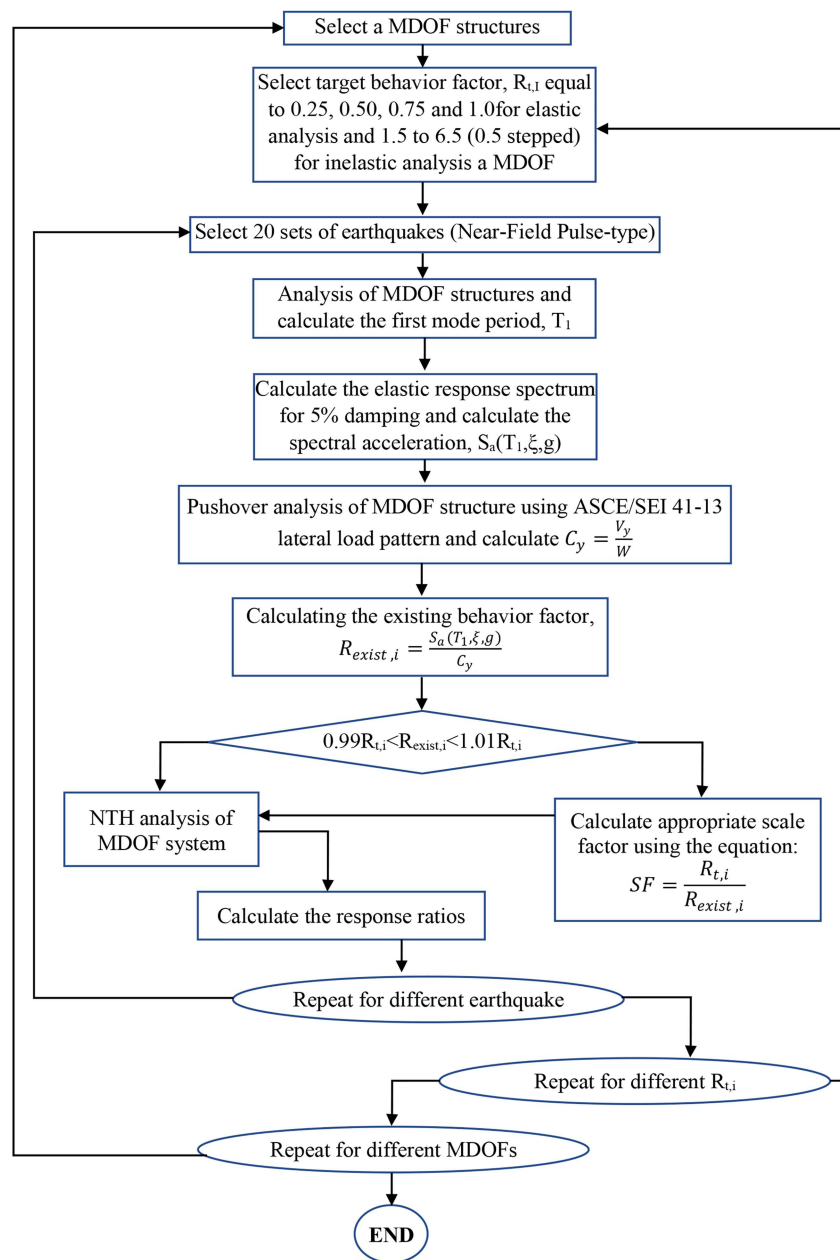


Figure 1. Flowchart of calculating response ratios.

1.5-6 in the inelastic analyses (with 0.5 increments). Afterward, the eigenvalues, and fundamental periods were determined. The elastic acceleration response spectra were also obtained considering a 5% inherent damping ratio. The yield base shear coefficient (C_y) was calculated using the ASCE/SEI 41-13 through pushover analysis of the MDOF structure. Note that the coefficient introduced as the behavior coefficient in this study ($R_{exist,i}$) was the ratio of the elastic spectral acceleration to the yield base shear coefficient of the MDOF structure (with damping ratio 5%). This complied with the FEMA440 definitions. Values of $R_{exist,i}$ and $R_{t,i}$ were compared, and if their difference was within 1%, the results of time history analyses

would be considered acceptable and, thus, the practical ratios were calculated. Otherwise, the records were multiplied by the $SF = R_{t,i} / R_{exist,i}$ (earthquake scale factor) and the time history analysis was repeated until the required convergence was obtained. Figure 1 depicts the steps of the process presented above.

4. Energy ratios for E-SDOF systems

Among different means of measuring and minimizing cumulative damage, the energy demand acting on the structure during earthquakes, as well as the structural response shown by the structure to absorb and dissipate energy, are of highest importance and efficiency.

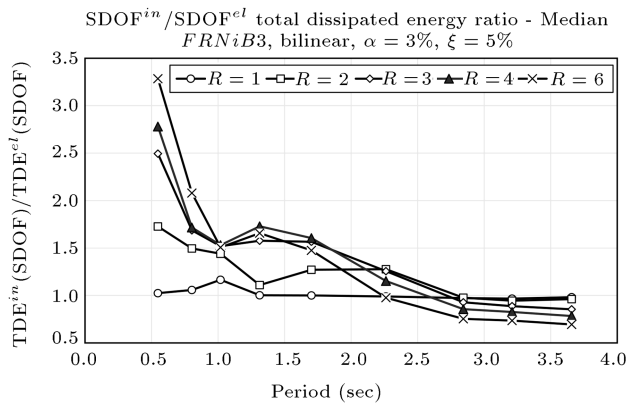


Figure 2. Ratio of inelastic to elastic total dissipated energy demands (TDE^{in}/TDE^{el}).

Hence, this study attempted to propose a method for estimating the peak energy and its relationship with the MDOF system. The energy response features resulting from the SDOF analyses are presented along with the pulse-type near-fault ground motions. These findings would be considered the basis for the distribution of energy in the MDOF structure. Further, energy demand is determined based on the intensity and duration of the earthquake. Hence, variations of R alter the intensity of an earthquake. However, in order to obtain results that are independent of the two aforementioned factors, the following diagrams are defined as dimensionless graphs and the applied energy ratios. These ratios are defined separately as follows.

4.1. Ratio of inelastic dissipated energy to elastic dissipated energy (TDE^{in}/TDE^{el})

The ratio of the mean total inelastic dissipated energy to total dissipated elastic energy (TDE^{in}/TDE^{el}) is presented in Figure 2. The ratio of dissipated energy is equal to the sum of damping and hysteretic energies at the end of the ground motion. Evidently, nonlinearity leads to a considerable increase in TDE^{in} within short periods. The estimated period corresponding to short and long periods is 1 second. For periods longer than 1 second, the increase in R (i.e. increased inelastic deformation) reduces the TDE^{in} demand. When the period is greater than 2.25 seconds, the calculated demand ratio is only weakly dependent on the period value and R . An acceptable correlation is seen between the abovementioned results and the study conducted by Seneviratna and Krawinkler [37]. Nevertheless, they used far-fault ground motion with the period range reported as 0.4 sec. They also concluded that the strain-hardening coefficient has a negligible effect on the total dissipated energy [37].

4.2. Ratio of Hysteretic Energy to Total Dissipated Energy Demand (HE/TDE)

In structures with low lateral strength, hysteretic energy dissipation is a mechanism that balances the

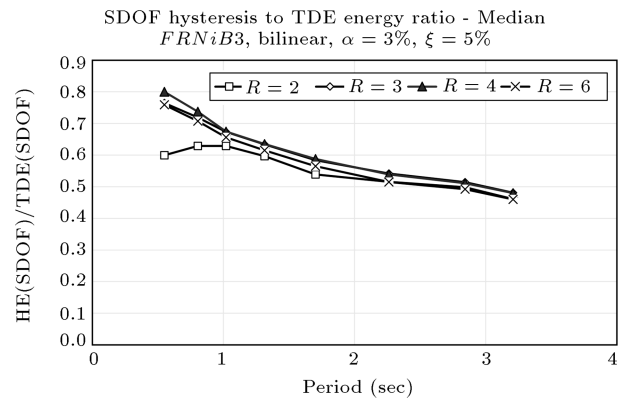


Figure 3. Ratio of hysteretic energy to total dissipated energy demands (HE/TDE).

energy imparted to a structure. This energy is normally associated with the extent of structural damage. Since TDE does not considerably depend on the R value (except in short-period structures), it is relevant to consider the fraction of TDE, which is hysteretic dissipated energy. Figure 3 illustrates the mean HE/TDE values for 10 near-fault ground motions. Owing to the stability of this index, this diagram conforms to the results obtained in other studies [37,38]. In short periods, the HE/TDE ratio grows with R , but for $T > 1.0$ sec., the effect of R on HE/TDE ratio diminishes. With an increase in the period, the HE/TDE ratio decreases linearly. This reduction is independent of the R value. A previous study concluded that the strain-hardening coefficient has a negligible effect on HE/TDE [37].

5. Relationship between energy demands of the MDOF and E-SDOF systems

As compared to strength and ductility demands, energy demand is a more accurate measure of the seismic response and structural performance. Hysteretic Energy (HE) can also properly measure cumulative damage. Although energy-driven design concepts, which are difficult to apply, have not become popular so far, it is still necessary to assess the dissipation of energy in structures, especially for structures that are subjected to a near fault pulse-like earthquakes. The results obtained from these assessments can contribute to the development of damage indices. The energy demand of SDOF systems has been addressed in many studies, which have led to several acceptable results. The study conducted by Fajfar and Vidic indicated that the ratio of HE (Hysteretic Energy) to Input Energy (IE) at the end of the ground motion is a fairly stable parameter [38]. In addition, since the input energy spectra are not very sensitive to the stored restoring force characteristics, IE is a suitable parameter to define the design earthquake [2]. However, only a few

studies have linked this feature to MDOF systems. As described earlier, the general method to estimate MDOF system energy using the total elastic dissipated energy of the SDOF system was considered the basis of this study. The current section discusses the qualitative and quantitative development of the correlation between the energy demands of the MDOF system and the E-SDOF system. The results of the nonlinear time history analyses and E-SDOF energy demand are used to calculate the maximum energy demand of the MDOF system. Note that the energy demand depends on the duration and intensity of the earthquakes.

5.1. Total Dissipated Energy (TDE) demand

Figure 4 displays the TDE ratio for an elastic system, in which energy dissipation is caused by 5% damping. The total dissipated energy demand (TDE) is the sum of damping and hysteretic energies. In this study, TDE is calculated at the end of the earthquake. Since, at the end of recording, the kinetic energy of the structure is small, TDE is very close to the total input energy. The TDE results are presented in Figures 5 and 6. The objective of the graphs is to allow evaluating the TDE in MDOF systems and as the basis of calculating

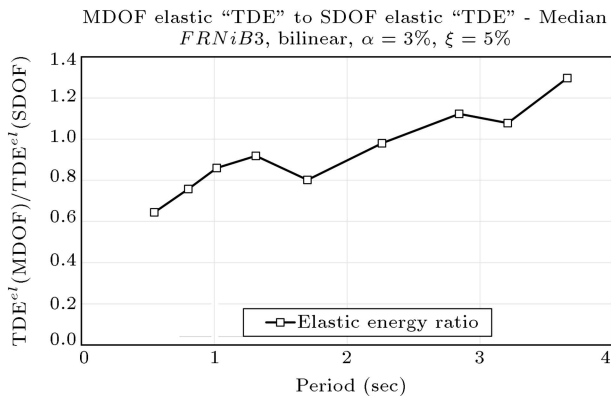


Figure 4. TDE ratio of elastic MDOF to elastic E-SDOF system.

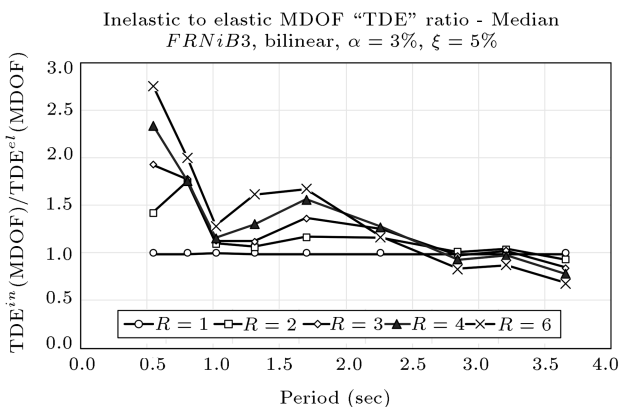


Figure 5. TDE ratio of inelastic MDOF to elastic MDOF system (relative and absolute TDE).

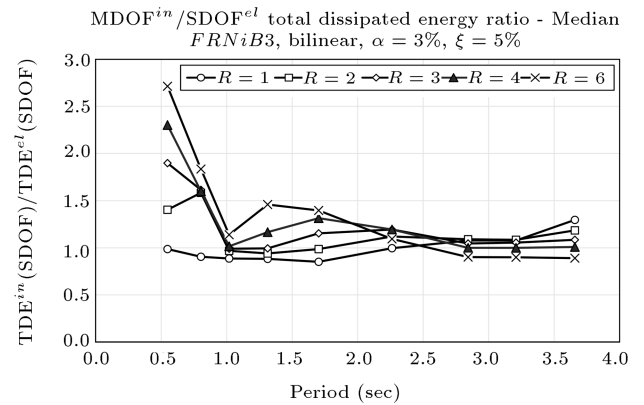


Figure 6. TDE ratio of inelastic MDOF to elastic E-SDOF system.

the TDE of the MDOF system via the SDOF energy spectrum.

The results are presented as the ratio of the TDE^{el} of the MDOF system to the TDE^{el} of the first mode E-SDOF system. The mean results are shown in Figure 4. The following observation can be made from the presented graphs:

- For short period structures, the TDE demand is, on average, 80% of the TDE demand of the first mode elastic E-SDOF system. This value is close to the effective modal mass of the first mode.
- The higher mode effect (MDOF effect) becomes important as the period prolongs. Hence, there is a significant increase in the TDE ratio.

Figure 5 depicts the absolute and relative TDE demand ratios of the inelastic MDOF system to the TDE demand of the elastic MDOF system. As can be observed, the pattern of this graph is very similar to the case of the E-SDOF system. Also, it is apparent that inelastic TDE is almost the same as the TDE of elastic systems, except for short period structures. This finding holds true even for high ductility values (i.e. R factors). In other words, there is a trade-off between damping and hysteretic energy.

Another parameter that could be used to assess the relationship between the TDE demand of MDOF and E-SDOF systems is the ratio of the TDE demand of the inelastic MDOF system to the elastic TDE demand of the E-SDOF system. It means that the total dissipated energy demand for the MDOF system is normalized by the TDE demand for the first mode E-SDOF system with the same R -value. The trend of this ratio over the period is illustrated in Figure 6. It can be seen that the pattern of this graph is very similar to the case of the E-SDOF system (Figure 2). It means that for long period structures, the TDE demand of the elastic E-SDOF system can be used as the TDE demand of the inelastic MDOF system. This is an

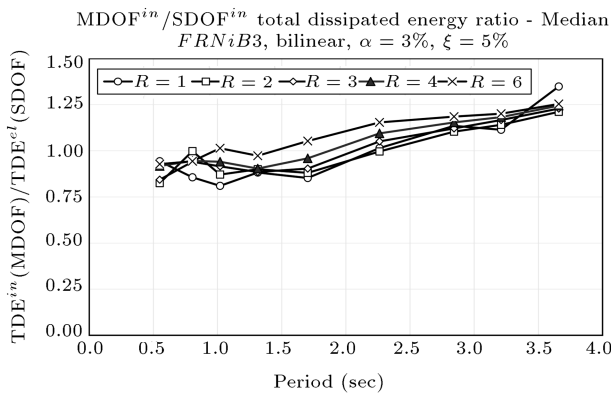


Figure 7. Higher mode effects (MDOF effects) on TDE demand.

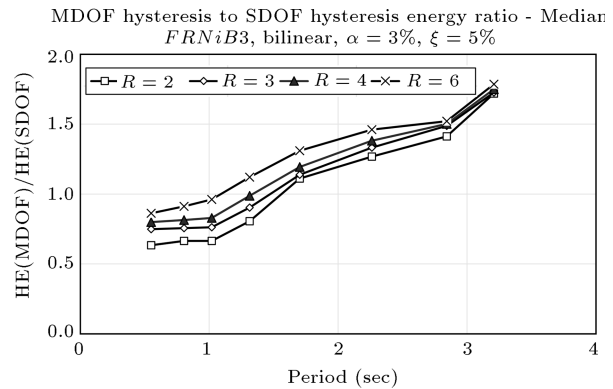


Figure 8. Higher mode effects (MDOF effects) on HE demand.

advantage since it is far easier to calculate the TDE demand for elastic E-SDOF. It means that for practical applications, while the TDE demand of the inelastic MDOF system is required, it can be estimated by the TDE demand of the elastic equivalent SDOF system, except for short period structures.

The inelastic TDE demand ratio of the MDOF system to the inelastic TDE demand ratio of the SDOF system for various R -values is shown in Figure 7. Similar to the previous sections, the mean results are presented in this section. For short-period structures, the TDE demand of the MDOF systems is smaller than that of the first mode E-SDOF system. As the period increases, the higher mode effects become significant, resulting in amplification of the TDE demand of the MDOF system. Further, the variations of the TDE ratio are almost independent of the design strength and nonlinearity level (R -value).

5.2. Hysteretic energy demand in MDOF systems

Hysteretic energy demand is a part of the input energy dissipated by the inelastic behavior of structural elements. Based on a study conducted by Gerami and Abdollahzadeh, the Hysteretic Energy (HE) can be considered a key factor in minimizing expected structural damage [39]. Hence, in this part of the paper, the mean HE energy of the 2D steel MRFs of the present study is depicted and discussed.

In this study, HE is defined as a total dissipated hysteretic energy at each plastic hinge. Figure 8 demonstrates the ratio of hysteretic energy dissipated energy in the MDOF system to the corresponding values obtained from an E-SDOF system considering various R values (level of nonlinearity). These curves indicate the effect of higher modes, degrees of freedom, and nonlinearity level on the HE demands. For short-period structures, the HE demand of the MDOF systems is smaller than that of the first mode E-SDOF system. As the period increases, the higher mode effects become significant, resulting in amplification of

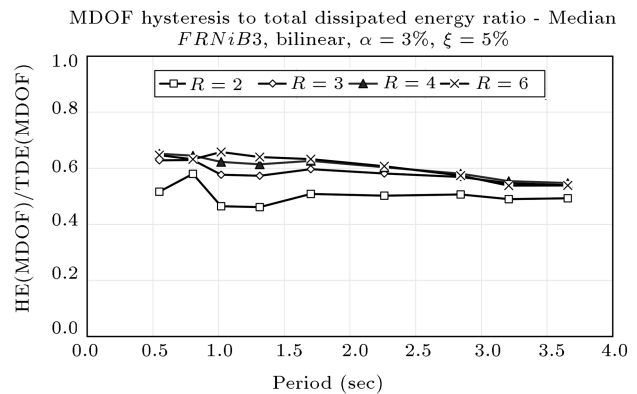


Figure 9. HE/TDE ratio of inelastic MDOF system.

the HE demand of the MDOF system. Further, for a constant period, the HE ratio is affected by the R -value (nonlinearity level). This effect becomes negligible for long period structures. In other words, increasing R reduces the effect of higher modes.

Both Figures 6 and 7 facilitate the estimation of the TDE demand of the frame structure using the SDOF system data under the conditions of pulse-type near-fault earthquakes with forward directivity.

As such, SDOF data can be used for this purpose. The HE to TDE demand ratio of MDOF structures is presented in Figure 9. The overall trend of the HE/TDE diagram is apparently similar to that of the HE/TDE for the corresponding E-SDOF system. Hence, the results of the E-SDOF system can be used to estimate the HE/TDE ratio for MDOF systems. As seen in Figure 9, the HE/TDE ratio in the MDOF system is weakly dependent on the R -value, except for $R = 2.0$.

5.3. Height-wise distribution of hysteretic energy demand (HE)

Previous sections mainly focused on the hysteresis (hysteretic energy) of the entire structure. However, the results obtained in these sections fail to give an accurate insight into the Hysteretic Energy (HE)

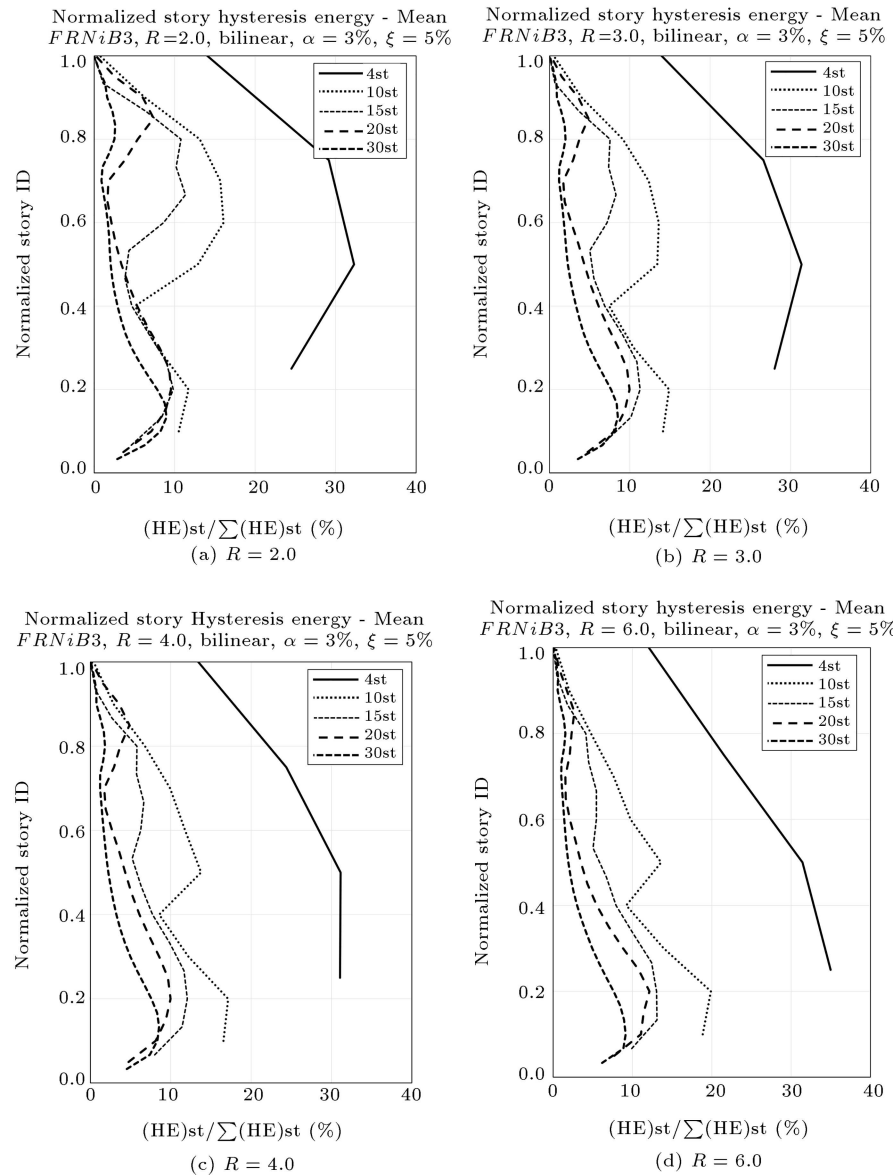


Figure 10. The story hysteretic energy distributed at height, $HE_{st,i}$ normalized by the total hysteretic energy for $R = 2, 3, 4, 6$ and 4-, 10-, 15-, 20-, and 30-story frames.

demands over the height of the structure. Hence, the concept of the story hysteretic energy demand ($HE_{s,i}$) is introduced. This parameter can be used to assess the distribution of structural damage over the height of the structure. The $HE_{s,i}$ is computed by integrating the story shear with respect to the inter-story drift. In order to gain a better statistical understanding of the accumulation of the story hysteretic energy, the story HE demand is normalized by the total dissipated hysteretic energy (HE_t), which shows the total HE energy on each story. Thus, the ratio can be defined as follows:

$$\frac{HE_{s,i}}{\sum HE_{s,i}} = \frac{HE_{s,i}}{HE_t} \quad (15)$$

Figures 10 and 11 reveal the mean values of the normalized story hysteretic energy over the height. Due to space limitation, graphs are shown only for $R = 2.0, 3.0, 4.0,$ and 6.0 . The vertical axis of all graphs is dimensionless in order to facilitate a simultaneous display of the results of different frames. To investigate the effect of R on the profile of the dissipated hysteretic energy, the trend of the $HE_{s,i}/HE_t$ ratio in each frame is plotted. The following observation can be made from the presented graphs:

- In structures where there is a high possibility of plastic hinge formation, accumulation of maximum energy demand is observed in the lower stories;
- In low- and mid-rise frames, the peak $HE_{s,i}/HE_t$

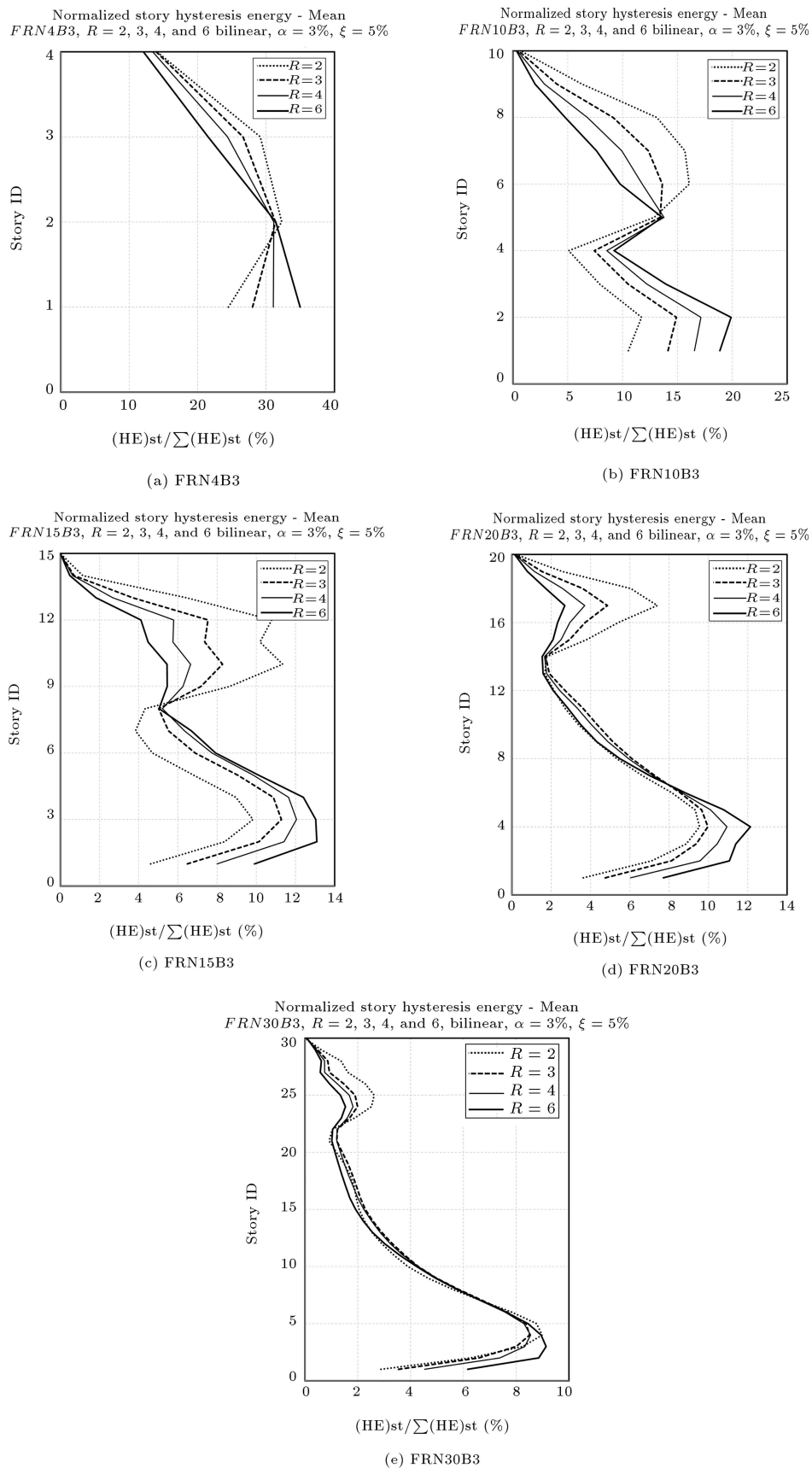


Figure 11. Story hysteretic energy distributed at height, $HE_{st,i}$ normalized by the total hysteretic energy for 4-, 10-, 15-, 20-, and 30-story frames.

ratio is influenced by the higher modes and locates at the upper stories for $R = 2.0$ and 3.0 . However, in high-rise frames (15 stories and more), the peak $HE_{s,i}/HE_t$ ratio occurs at the lower floors due to the nature of near field motion and dynamic instability. Further, for the low- and mid-rise models, while the R -value increases, the $HE_{s,i}/HE_t$ ratio accumulates in the bottom stories. It means that the effect of the higher modes declines while the R increases;

- In the upper stories, the $HE_{s,i}/HE_t$ ratio diminishes with an increase in R . On the other hand, increasing R -value enhances the $HE_{s,i}/HE_t$ ratio in the bottom stories due to the P - Δ effects and dynamic instability. In high-rise frames, almost one-third of the height has a similar $HE_{s,i}/HE_t$ ratio profile and is not significantly sensitive to R variations.

5.4. Contribution of hysteretic and damping energy for MDOF system

If an earthquake does not damage a structure, the residual strain and kinetic energies are dissipated by means of damping during its free vibrations. Subsequent to the free vibration of the structure, the sum of the damping and hysteretic energies equals the earthquake total input energy. The following equations are defined to calculate the kinetic energy (E_k), damping energy (E_ξ), and the sum of elastic and inelastic strain energies ($E_{se} + E_K$) of the MDOF structure [5]:

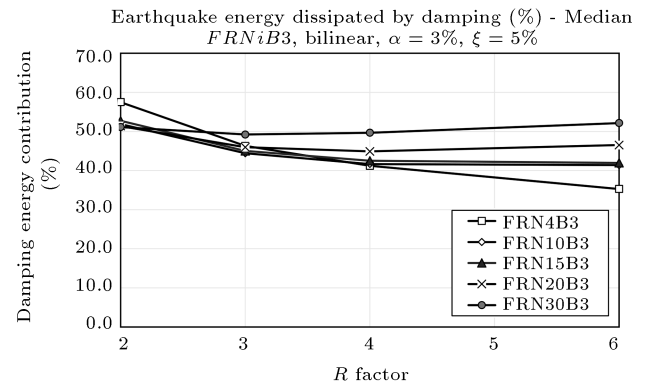
$$E_K = \int \{\dot{u}\}^T [\mathbf{m}] \{\dot{u}\} dt, \quad (16)$$

$$E_\xi = \int \left(\{\dot{u}\}^T [\mathbf{c}] \{\dot{u}\} \right) dt, \quad (17)$$

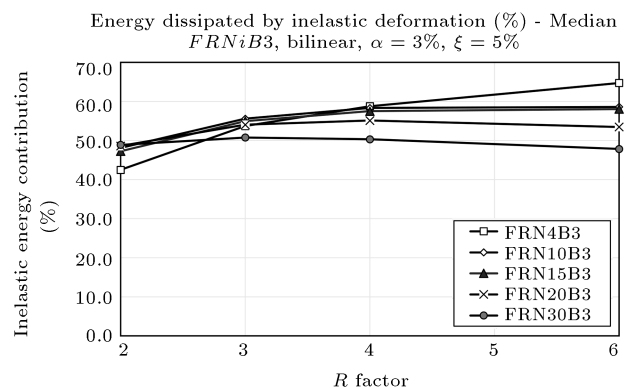
$$E_{se} + E_H = \int \{\dot{u}\}^T [\mathbf{K}] \{u\} dt. \quad (18)$$

The strain energy consists of elastic and inelastic strain energy (i.e. hysteretic energy), as shown by Eq. (18). Elastic strain energy is the part of earthquake input energy, which is stored as elastic strain in structural elements. This stored energy is transformed to damping and kinetic energy during free vibrations. Hysteretic energy is the sum of the energy dissipated due to the inelastic deformations of the structural elements [5]. Figure 12 displays the percentage of energy dissipated due to damping and inelastic deformations along with the input energies for various R -values and three-span models at the end of vibrations.

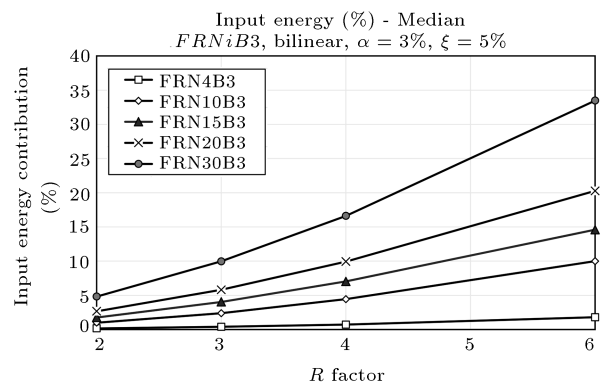
According to Figure 12, an increase in R decreases the contribution of damping energy. Meanwhile, the degree of reduction depends on the structure height. For instance, in the case of $R = 6$, with an increase



(a) Damping energy dissipated



(b) Inelastic deformation energy dissipated



(c) Input energy

Figure 12. Variations of damping, hysteretic, and input energies contribution for various R -values.

in the height of a structure, the share of damping dissipated energy increases. The aforementioned effect is due to accumulation of the peak nonlinear demands of the structure in the lower stories of high-rise buildings under pulse type near fault ground motions. This has been confirmed in previous studies, such as those of Gerami and Abdollahzadeh [40]. Hence, as the contribution of higher modes of vibration declines, the number of inelastic elements decreases and so the share of damping energy increases to balance the dissipated

Table 5. Comparison of the average dissipated energy by damping and hysteresis for various R -values.

Structural model	R	Earthquake	Total dissipated energy	
		Input energy (kJ)	Damping (%)	Hysteresis (%)
FRN4B3	2	178	57.5	42.5
	3	399	46.3	53.7
	4	722	41.2	58.8
	6	1802	35.3	64.7
FRN10B3	2	1001	51.9	48.1
	3	2389	44.4	55.6
	4	4439	41.7	58.3
	6	9994	41.4	58.6
FRN15B3	2	1765	52.7	47.3
	3	4040	45.0	55.0
	4	7039	42.5	57.5
	6	14597	42.0	58.0
FRN20B3	2	2669	51.4	48.6
	3	5813	46.0	54.0
	4	9928	44.9	55.1
	6	20265	46.5	53.5
FRN30B3	2	4816	51.1	48.9
	3	9967	49.2	50.8
	4	16608	49.7	50.3
	6	33462	52.2	47.8

energy. However, in the case of $R = 2.0$, more elements are transitioned to the inelastic phase due to the effect of higher modes over the height of the structure. The findings of this paper are in agreement with the results of Gerami and Abdollahzadeh [40] for small R -values.

Table 5 compares the damping and hysteretic dissipated energy where the contribution of the structure nonlinearity to the dissipated energy can be studied. The results listed in Table 5 indicate that for the lower nonlinearity level (i.e. $R = 2$) in low and mid-rise structures, the damping energy is almost 10% more than the hysteretic energy. However, this trend is reversed with an increase in R . It means, while R -value grows, the contribution of damping energy diminishes and the share of hysteretic energy increases. Further, with an increase in the number of stories (e.g. in the FRN30B3 frame), the variations of R do not affect the contribution of the dissipated hysteretic and damping energies. In other words, the effects of both energy dissipation mechanisms are the same.

6. Conclusion

Establishing a rational relationship between MDOF and corresponding SDOF energy demands, especially for pulse-type near-fault ground motion, was a major objective of this paper, which, therefore, distinguishes

the current work from previous studies. The proposed correlation ratios help in quick evaluation of different energy demands for steel MRFs without performing nonlinear time history analysis and with only having an equivalent SDOF system. Thus, different energy demands, such as Total Dissipated Energy (TDE, elastic and inelastic), the Hysteretic dissipated Energy (HE), Damping Energy (DE), and Elastic Strain Energy (ESE), have been considered. To this end, 3-span with 4-, 10-, 15-, 20-, and 30-story steel MRFs were defined. Nonlinear dynamic analyses were conducted under 10 near-fault earthquakes with forward directivity. In order to propose practical energy ratios, the inelastic to elastic total dissipated energy ratio and the dissipated hysteretic energy to the total dissipated energy ratio for both MDOF and E-SDOF systems were calculated and presented. Further, the energy demand of the MDOF system was normalized with the corresponding energy demand of the E-SDOF system to consider the effects of higher modes and degrees of freedom. Finally, the height-wise hysteretic energy demand and the contribution of hysteretic and damping energy for steel MRFs were evaluated. According to the results of the analyses, the following findings can be concluded:

- The TDE^{in}/TDE^{el} ratio resulted for the E-SDOF system was weakly dependent on the period and

nonlinearity, except for periods shorter than 1 sec. The same finding held also true for the HE/TDE ratio. The trend of the HE/TDE ratio for long period systems depended on the earthquake energy content substantially. For instance, if the decline rate of the mean response spectrum was large within a longer period, the HE/TDE ratio would diminish more rapidly;

- The TDE demand of the elastic MDOF structure was on average equal to 80% of the TDE demand of the corresponding elastic E-SDOF system. With an increase in the period, due to the MDOF effect, the TDE ratio ($TDE_{MDOF}^{el}/TDE_{SDOF}^{el}$) increased drastically;
- Evaluation of ($TDE_{MDOF}^{in}/TDE_{MDOF}^{el}$) ratio demonstrated that the dissipated energy in the nonlinear structure is equal to dissipation of energy due to damping in the elastic system, except for short period frames. It means a balance exists between the damping and hysteretic energy;
- The ratio of ($TDE_{MDOF}^{in}/TDE_{SDOF}^{el}$) shows that the effect of MDOF increases the corresponding TDE of the inelastic MDOF system. On the other hand, for short period models, the elastic TDE of E-SDOF is an acceptable estimation. This ratio is almost independent of the design strength and R -value;
- The trend of the HE/TDE ratio caused the MDOF structure to be similar to the corresponding E-SDOF ratio. Hence, the E-SDOF system ratio is practical for the MDOF system;
- The height-wise distribution profile of the normalized median of maximum values of story hysteresis energy depends on the nonlinearity level (R -value) and structure period (height). For instance, shorter period structures with lower R -values provide peak normalized hysteresis energy located at the upper floors. As R -value increased, the median of maximum values of story hysteresis energy transferred to the bottom stories and the effect of higher modes disappeared. This finding is observable for long period models with different R -values.

A balance between damping and hysteretic energy was recognizable in all steel MRFs. For instance, increasing the value of R led to reduced damping energy contribution. Further, for short period structures, the contribution of hysteretic energy was greater than that of the damping energy.

Nomenclature

C_y	Yield base shear coefficient
E_{AI}	Absolute input energy

E_H	Plastic strain energy
E_K	Absolute kinetic energy
E_{KR}	Relative kinetic energy
E_{RI}	Relative input energy
E_s	Elastic strain energy
E_ξ	Damping energy
$E - SDOF$	Equivalent single degree of freedom system
ϕ_1	First mode shape vector
φ_{r1}	The value of φ_1 at the roof and equal to $R_{t,i}/R_{exist,i}$
HE	Hysteretic Energy
$HE_{s,i}$	Story hysteretic energy demand
HE_t	Total dissipated hysteretic energy
HE/TDE	Ratio of hysteretic energy to total dissipated energy demand
IE	Input Energy
m_1^*	Effective modal mass
MDOF	Multi Degree Of Freedom system
MPA	Modal Pushover Analysis
MRF	Moment Resistance Frame
PBPD	Performance-Based-Plastic Design
PGV	Peak Ground Velocity
R	Behavior factor
$R_{exist,i}$	Behavior coefficient in this study
$R_{t,i}$	Target behavior coefficient
SDOF	Single Degree Of Freedom system
SF	The earthquake Scale Factor
TDE	Total Dissipated Energy
TDE^{el}	Elastic dissipated energy
TDE^{in}	Inelastic dissipated energy
TDE^{in}/TDE^{el}	Ratio of inelastic dissipated energy to elastic dissipated energy

References

1. Haddad-Shargh, F. and Hosseini, M. "An optimal distribution of stiffness over the height of shear buildings to minimize the seismic input energy", *Journal of Seismology and Earthquake Engineering*, **13**(1), pp. 25–32 (2011).
2. Uang, C.M. and Bertero, V.V. "Evaluation of seismic energy in structures", *Earthquake Engineering: Structural Dynamics*, **19**(1), pp. 77–90 (1990).
3. Housner, G.W. "Limit design of structures to resist earthquakes", In: *Proceedings of 1st World Conference on Earthquake Engineering*, **5**, Oakland, Calif, USA, pp. 1–13 (1956).
4. Leelataviwat, S., Goel, S.C., and Stojadinovi'c, B. "Toward performance-based seismic design of structures", *Earthquake Spectra*, **15**(3), pp. 435–461 (1999).

5. Khashaee, P., Mohraz, B., Sadek, F., et al. "Distribution of earthquake input energy in structures", Tech. Rep. NISTIR 6905, United States Department of Commerce Technology Administration, National Institute of Standards and Technology, Gaithersburg, Md, USA (2003).
6. Goel, S.C., Liao, W.C., Bayat, MR., et al. "Performance-based plastic design (PBDP) method for earthquake-resistant structures: an overview", *Struct Des Tall Spec*, **19**(1–2), pp. 115–37 (2010).
7. Banihashemi, M.R., Mirzagoltabar, A.R., and Tavakoli, H.R. "Development of the performance based plastic design for steel moment resistant frame", *Int J Steel Struct*, **15**(1), pp. 51–62 (2015).
8. Sahoo, D.R. and Chao, S. "Performance-based plastic design method for buckling-restrained braced frames", *Eng Struct*, **32**(9), pp. 2950–2958 (2013).
9. Wongpakdee, N., Leelataviwat, S., Goel, S.C., et al. "Performance-based design and collapse evaluation of buckling restrained knee braced truss moment frames", *Eng Struct*, **60**, pp. 23–31 (2014).
10. Heidari, A. and Gharehbaghi, S. "Seismic performance improvement of special truss moment frames using damage and energy concepts", *Earthq Eng Struct Dyn*, **44**(7), pp. 1055–1073 (2015).
11. Kharmale, S.B. and Ghosh, S. "Performance-based plastic design of steel plate shear walls", *J Constr Steel Res*, **90**, pp. 85–97 (2013).
12. Connor, J.J., Wada, A., and Iwata, M., et al. "Damage-controlled structures. I. Preliminary design methodology for seismically active regions", *J Struct Eng*, **123**(4), pp. 423–431 (1997).
13. Vargas, R. and Bruneau, M. "Analytical response and design of buildings with metallic structural fuses. I", *J Struct Eng*, **135**(4), pp. 386–393 (2009).
14. Ke, K., Yam, MCH., and Ke, S. "A dual-energy-demand-indices-based evaluation procedure of damage-control frame structures with energy dissipation fuses", *Soil Dyn Earthq Eng*, **95**, pp. 61–82 (2017).
15. Du, B., He, Z., Wu, Y., and Pan, F. "A compatible energy demand estimate considering code-specified design spectra", *Soil Dynamics and Earthquake Engineering*, **137**, p. 106273 (2020).
16. Yang, T.Y., Neitsch, J., Al-Janabi, M.A.Q., and Tung, D.P. "Seismic performance of eccentrically braced frames designed by the conventional and equivalent energy procedures", *Soil Dynamics and Earthquake Engineering*, **139**, p. 106322 (2020).
17. Guo, W., Du, Q., Huang, Z., et al. "An improved equivalent energy-based design procedure for seismic isolation system of simply supported bridge in China's high-speed railway", *Soil Dynamics and Earthquake Engineering*, **134**, p. 106161 (2020).
18. Oh, S.H., Shin, S.H., and Bagheri, B. "Stability evaluation of the acceleration and energy response spectra", *Soil Dynamics and Earthquake Engineering*, **123**, pp. 124–143 (2019).
19. Zhou, Y., Song, G., Huang, S. et al. "Input energy spectra for self-centering SDOF systems", *Soil Dynamics and Earthquake Engineering*, **121**, pp. 293–305 (2019).
20. Zhou, Y., Song, G., and Tan, P. "Hysteretic energy demand for self-centering SDOF systems", *Soil Dynamics and Earthquake Engineering*, **125**, p. 105703 (2019).
21. Yang, T.Y., Tung, D.P., and Li, Y. "Equivalent energy design procedure for earthquake resilient fused structures", *Earthquake Spectra*, **34**(2), pp. 795–815 (2018).
22. Vahdani, R., Gerami, M., and Vaseghinia, M.A. "Structural damping and displacement ductility effects on input energy spectrum of earthquake", *Journal of Structural and Construction Engineering*, **5**(2), pp. 5–21 (2017) (in Persian).
23. Benioff, H. "Mechanism and strain characteristics of the white wolf fault as indicated by the aftershock sequence", *Calif. Div. Mines Bull*, **171**, pp. 199–202 (1955).
24. Mahin, S.A., Bertero, V.V., Chopra, A.K., et al. "Response of the olive view hospital main building during the San Fernando earthquake", *Earthquake Engineering Research Center*, University of California, Berkeley, Technical Report, 1976-10 (1976).
25. Bertero, V.V., Mahin, S.A., and Herrera, R.A. "A seismic design implications of near-fault San Fernando earthquake records", *Earthquake Engineering and Structural Dynamics*, **6**(1), pp. 31–42 (1978).
26. Hall, J.F., Heaton, T.H., Halling, M.W., et al. "Near-source ground motion and its effects on flexible buildings", *Earthquake Spectra*, **11**(4), pp. 569–605 (1995).
27. Krawinkler, H., Anderson, J., Bertero, V., and Theil, Jr. C. "Steel buildings", *Earthquake Spectra*, **12**(S1), pp. 25–47 (1996).
28. Makris, N. and Black, C.J. "Dimensional analysis of bilinear oscillators under pulse-type excitations", *Journal of Engineering Mechanics*, **130**(9), pp. 1019–1031 (2004).
29. "DHUD-Part6: Applied loads on buildings", Department of Housing and Urban Development, *Iranian National Building Code-Part 6*, third edition (2014) (in Persian).
30. "BHRC-PN 253: Iranian code of practice for seismic resistant design of building", *Iranian Building Codes and Standards*, forth revision (2014) (in Persian).
31. ASCE/SEI 7: *Minimum Design Loads for Buildings and Other Structures*, American Society of Civil Engineers, USA (2016).
32. Computers and Structures, Inc "Etabs 2016-extended 3D analysis of building systems, nonlinear", Berkeley, California 94704, USA.
33. ANSI/AISC 360-10: *Specification for Structural Steel Buildings*, American Institute of Steel Construction, Chicago (2010).

34. McKenna, F. “OpenSees: a framework for earthquake engineering simulation”, *Computing in Science: Engineering*, **13**(4), pp. 58–66 (2011).
35. Baker, J. “Quantitative classification of near-field ground motion using wavelet analysis”, *Bulletin of the Seismological Society of America*, **97**(5), pp. 1486–1501 (2007).
36. Chopra, A.K. and Goel, R.K. “A modal pushover analysis procedure for estimating seismic demands for buildings”, *Earthquake Engineering: Structural Dynamics*, **31**(3), pp. 561–582 (2002).
37. Seneviratna, G. and Krawinkler, H., *Evaluation of Inelastic MDOF Effects for Seismic Design*, John A. Blume Earthquake Engineering Center (1997).
38. Fajfar, P. and Vidic, T. “Consistent inelastic design spectra hysteretic and input energy”, *Earthquake Engineering: Structural Dynamics*, **23**(5), pp. 523–537 (1994).
39. Gerami, M. and Abdollahzadeh, D. “Estimation of forward directivity effect on design spectra in near field of fault”, *Journal of Basic and Applied Scientific Research*, **2**(9), pp. 8670–8678 (2012).
40. Gerami, M. and Abdollahzadeh, D. “Numerical study on energy dissipation of steel moment resisting frames under effect of earthquake vibrations”, *Advances in Acoustics and Vibration*, **2014**, pp. 1–13 (2014).

Biographies

Seyed Abdonnabi Razavi received BS and MS degrees in Civil Engineering from the Islamic Azad University, in 2005 and 2007, respectively and is currently a PhD Candidate at the Ahvaz branch of the Islamic Azad University. His research interests include steel structure seismic assessment, evaluation of structures against progressive collapse, extension of the Hybrid Force/Displacement design method (HFD) and optimization of seismic design correlations using artificial Neural Networks (ANNs). He is also now working

as a member of the faculty of the Civil Engineering Department at the Islamic Azad University.

Navid Siahpolo received his BS degree in Civil Engineering from Shahid Chamran University of Ahvaz, Iran, in 2003, his MS degree in Structural Engineering from the Persian-Gulf University, Bushehr, Iran, in 2006, and his PhD degree in Earthquake Engineering at Semnan University, Iran, in 2015. His dissertation was entitled “The effect of near-fault pulse-like earthquakes on frame structures and the development of practical equations for quick assessment and design of steel moment resistant structures named Hybrid Force-Displacement Design (HFD)”. He has published more than 40 articles in peer-reviewed journals, as well as presented around 70 scholarly papers in various national and international conferences (in Persian and English). So far, he has published two books entitled: *Practical Fundamentals of Earthquake Engineering and Practical Earthquake Engineering*, in Farsi. Dr. Siahpolo is Assistant Professor of Civil Engineering at the Institute for Higher Education, ACECR, Khouzestan, Iran.

Mehdi Mahdavi Adeli received his MS degree in Earthquake Engineering and his PhD in Structural Engineering from Amirkabir University of Technology, Tehran, Iran. He is currently Assistant Professor in the Civil Engineering Department of the Islamic Azad University, Ahvaz branch. Beside academic activities and teaching some specialized courses in structural engineering, he also has undertaken some administrative responsibilities, acting as Deputy of Technical and Development Affairs at the Central Organization of the Islamic Azad University. His research interests and expertise include reliability analysis of structures and performance-based earthquake engineering. So far, he has supervised more than 200 MS degree students and 5 PhD candidates.